

Effect of low energy proton and He particle irradiation on CsPbBr₃ material

H. Y. Mei^a, H. T. Wu^a, R. X. Yao^a, L. Y. Zhao^a, X. Y. Zheng^a, F. Liu^{a,c},
I. H. Wen^a, S. X. Sun^{a,b,c*}

^a*Henan Provincial Key Laboratory of Smart Lighting, School of Information Engineering, Huanghuai University, Zhumadian 463000, China*

^b*Chongqing Institute of Microelectronics Industry Technology, UESTC, Chongqing 401331, China*

^c*Henan International Joint Laboratory of Behavior Optimization Control for Smart Robots*

In this paper, the effect of proton and He particle bombardment in CsPbBr₃ material was investigated by the Monte Carlo simulation including ion range, backscattering, vacancies and sputtering yield. The energies of proton and He particle varied from 50 keV to 180 keV and the particle incidence angles increased from 0° to 89.9°. The calculated results showed that with the increase of incidence energies, the range and vacancies increased, and the backscattering ions and sputtering yield reduced for proton and He particle. Meanwhile, the vacancies, backscattering ions and sputtering yield induced by He particle were much more proton at the same energy. With the increase of incidence angles, the range and vacancies were reduced, and the sputtering yield increased for proton and He particle. Also, it is obvious that the effects of He particle on CsPbBr₃ material were much more serious than proton.

(Received September 17, 2021; Accepted January 13, 2022)

Keywords: CsPbBr₃, Particle irradiation, Backscattering ions, Sputtering yield

1. Introduction

Due to the excellent photoelectric performance for the inorganic perovskite material, it is very suitable for application in optoelectronic devices such as light-emitting diodes, solar cells, detectors and lasers, which have attracted extensive attention of researchers[1-3]. With the rapid development of commercial space programs, solar cells have been widely applied in kinds of space equipment[4]. After nearly ten years of development, great progress has been made in perovskite solar cells. Recently, the energy conversion efficiency of solar cells based on perovskite materials have exceeded 20%[5]. Therefore, it has become a competitive candidate for remote power generation on unmanned aerial vehicles as well as spacecraft.

When perovskite solar cells are used in complex space environment, they will unavoidably be affected by charged particles in space[6]. Incident particles interact with perovskite materials

* Corresponding author: sunshuxianga@126.com

<https://doi.org/10.15251/DJNB.2022.171.39>

which will cause lattice atoms to shift and affect the carrier life, and led to reducing the efficiency of solar cells, ultimately leading to spacecraft orbital service time being reduced due to insufficient power[7]. Among these particles, proton and He are the most principal particles affecting devices[8], which deriving from galactic cosmic radiation and solar flares. Therefore, it is necessary to have a better understanding of the proton and He irradiation effect on perovskite materials.

Due to the strong stability, the perovskite material of CsPbBr₃ has attracted extensive attention, and most of researches are focused on enhancing the performance of CsPbBr₃[9]. Ding et al.[10] applied doping Zn²⁺ to CsPbBr₃, the quantum efficiency and stability were improved while the fluorescence intensity of the material was maintained, and PLQY increased from 32% to 36%. Akkerman et al.[11] was prepare solar cells with the CsPbBr₃ quantum dots and achieved photoelectric conversion efficiency of more than 5%. However, the comprehensive assessment of the irradiation effects on CsPbBr₃ has not been undertaken until now. Therefore, the irradiation effects of CsPbBr₃ induced by proton and He are of significant importance to prompt the pervasive application of perovskite solar cells in space environment.

In this work, the effects of proton and He bombardment on CsPbBr₃ at energies ranges from 50 keV to 180 keV and incidence angle ranges from 0 to 89.9 was investigated by using Monte Carlo SRIM software, such as ion range, backscattering, vacancies and sputtering yield. This research will help interpreting and understanding the damage mechanism of perovskite materials under irradiation, and might help the perovskite materials move one step closer to space applications.

2. Simulations

In this work, the open-source Monte-Carlo program SRIM was used to investigate the irradiation effects on material of CsPbBr₃. SRIM software is a program to simulate the interaction between ion beam and materials[12,13]. It can simulate the motion of incident particles, quickly calculate the depth of injection of particles with a certain energy into the sample, the distribution of incident particles in the sample and the damage caused by incident particles to the sample. The collision between the incident particle and the target nucleus of the material is described by two-body collision[14]. The motion of the incident particle in the matrix is regarded as a series of independent collisions with the matrix atoms, and each independent collision scattering is solved by numerical integration.

In this study, the parameters of the CsPbBr₃ was shown in Table 1. The incident energy of H and He was ranged from 50 keV to 180 keV, and the incident angle was varied from 0° to 89.9°. To ensure that all incident particles remain in the target, the thickness of CsPbBr₃ was set as 5 um. The total number of incident particle was set 10⁴ in each simulation[15] and well avoid higher fuctuations and to obtain better statistical values. For calculating the backscattering particles, number of vacancies and ion range, and the “Detailed Calculation with full Damage Cascades” mode was selected. For calculating the sputtering yield, the “Monolayer Collision Steps/Surface Sputtering” mode was used[16].

Table 1. Parameters input used in simulation[17].

	CsPbBr ₃
Total number of ions	10 ⁴
Mass density (g/cm ³)	4.56
Thickness(um)	5
Surface binding energy (eV)	Cs:0.81 Bb:2.03 Br:2
Lattice binding energy (eV)	Cs:3 Bb:3 Br:3
Displacement energy (eV)	Cs:25 Bb:25 Br:25

3. Results and discussion

When the energetic particles pass through the material, it will transfer their energy to the material atoms and terminate at a certain point in a material. Figure 1 shows the ranges of H and He in CsPbBr₃ with different incident energies. It can be seen that the ranges of H and He were both increased with the increase of the incident energy. Within 50-180 keV, the H ion range in CsPbBr₃ was increased from 5398.5 Å to 18215 Å and the He ion range in CsPbBr₃ was increased from 4256.5 Å to 11319 Å. Also, it is obvious that the range of H ion was larger than the He ion at all energies. This is because the focusing effect of ion implantation becomes obvious with the increase of energy, and the kinetic energy of ion beam increases, so the projection range increases.

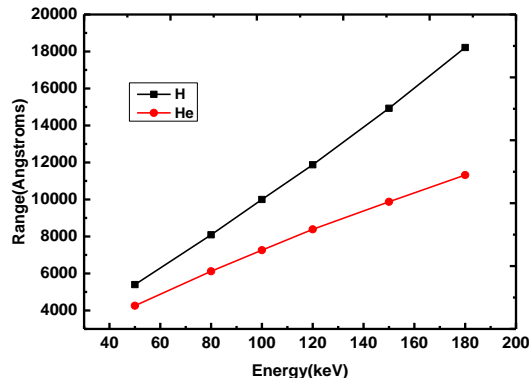


Fig. 1. The ranges of H and He in CsPbBr₃ with different incident energies.

Figure 2 (a) and (b) shows the distribution of H and He ion concentration in CsPbBr₃ with different energies. It can be seen that the peak ion concentration decreases at the projection range with the increase of energy. This is mainly due to the change of incident direction of some ions caused by the collision between ions and target atoms, and the continuous loss of kinetic energy of moving ions in the incident process causes some ions to gradually stop moving instead of stopping at the projection range, resulting in the decrease of peak ion concentration. In addition, the peak width is widened which mean that the standard deviation of range become larger with the increase of incident energy. That is to say, the dispersion of range will be increased.

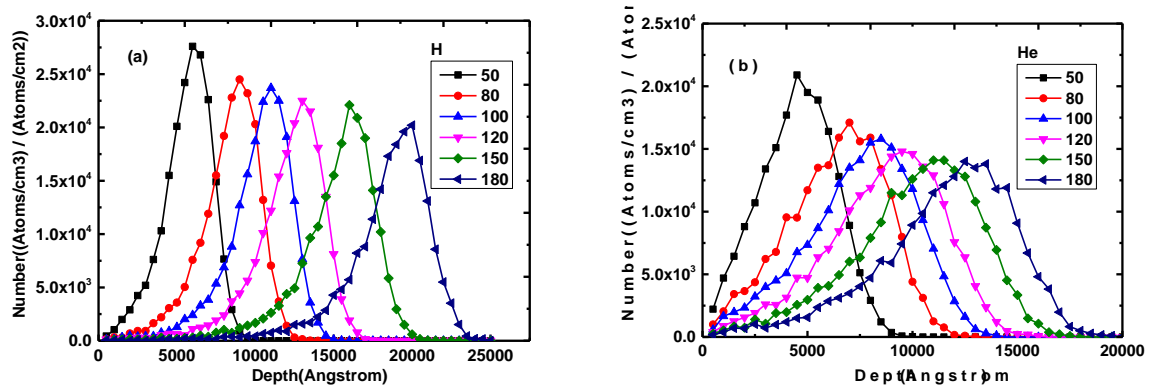


Fig. 2. The distribution of H and He ion concentration in CsPbBr₃ with different energies.

Figure 3 shows the variation of backscattering ions with different energies. With the increase of incident energy, the number of backscattering ions got decreased. With in 50-180 keV, the number of backscattering ions for H ion decreased from 141 to 25 and the number of backscattering ions for He ion are decreased from 689 to 132. Also, it is obvious that the number of backscattering ions for He ion was larger than H ion at all energies. With the increase of incident energy, depth of entry into material is increased, more energy was transferred to the target atom and the reflected H and He ion is not enough energy to escape from the surrounding atomic potential field which led to decreasing backscattering ions. However, the depth of He ion is much smaller and has a high chance of being reflected onto the surface of the material. Therefore, the number of backscattering ions for He ion were more at the same incident energy.

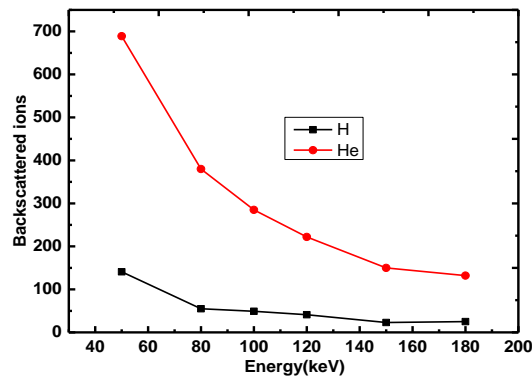


Fig. 3. The variation of backscattering ions with different energies.

When ion irradiates the material, collision cascade will be occurred along the track and vacancies defects will be created. The variation of vacancies induced by H and He ion with different energies was shown in Figure 4. It can be concluded that total vacancies induced by H and He ion increase by increasing the incident energy. At energy equal to 50 keV, the number of vacancies induced by H and He are 7.3 and 97.3, respectively. At energy equal to 180 keV, the number of vacancies induced by H and He are 11.8 and 145.3, respectively. This is mainly due to He ion is heavier than the H ion, and movement speed of He ion is smaller in the material, increasing the chance of a collision with the target atom which led to creating more vacancies.

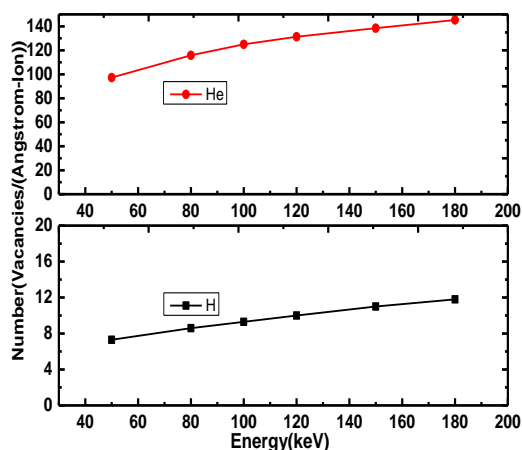


Fig. 4. The variation of vacancies induced by H and He ion with different energies.

Figure 5 shows the variation of the sputtering yield for the H and He ions at different ion energies. It can be seen from the figure that when the energy of incident ions increases, the sputtering yield generally decreases and the sputtering yield of He ion is higher than that of H ion. As the energy increases, the projection range of ions also increases. When ions incident deeper into the target, displaced atoms deep within the target material cannot escape from the surface of the material, leading to decreasing the sputtering yield.

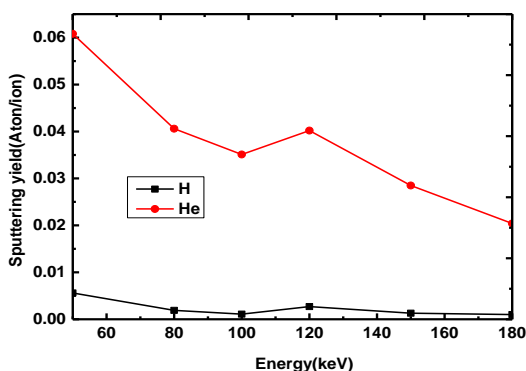


Fig. 5. The variation of the sputtering yield for the H and He ions at different ion energies.

The relation between ion range and ion incident angle for CsPbBr₃ using H and He ion at incident energy of 100 keV is shown in Figure 6. It is found that the ion range decreases by increasing the incident angle. At normal incidence, the ion range was farthest for H and He ion. Figure 7 (a) and (b) shows the distribution of H and He ion concentration in CsPbBr₃ with different incident angles at incident energy of 100 keV. As can be seen from the figure, the peak value of ion concentration decreases with the increase of incident angle and he ion projection range corresponding to the peak of ion concentration also decreases. Under the transverse diffusion effect, the more displaced target atoms generated after the collision with incident ions increases when the increase of incident angle. Therefore, the incident ion would transfer more energy through the inelastic collision between the target atom, which makes the ion stop moving earlier and stay closer to the surface of material. Moreover, the He ion is more heavier and led to the smaller range.

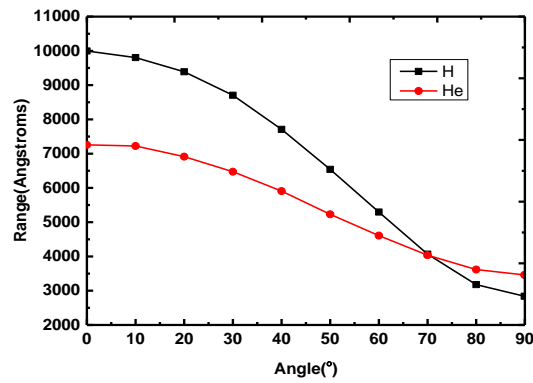


Fig. 6. The ranges of H and He in CsPbBr₃ with different incident angles.

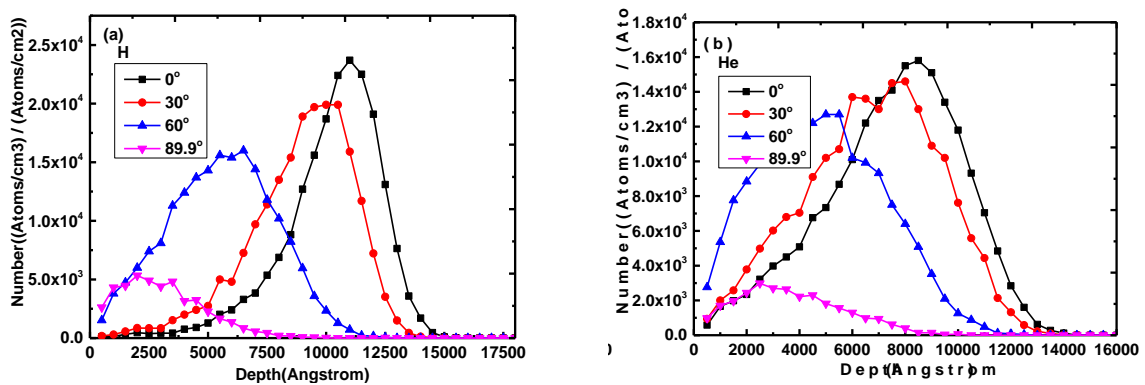


Fig. 7. The distribution of H and He ion concentration in CsPbBr₃ with different incident angles.

Figure 8 plots the number of vacancies defects produced in CsPbBr₃ with respect to the different incident angles for H and He ion at 100 keV. It is discovered that the variation trend of vacancies for H and He ion shows the similar changes except that the calculated values are different. The number of vacancies were gradually decreased with the increase of the incident angle. As the incident angle increases, the energy transferred to the target atom by the incident ion decrease, so the degree of damage formed is reduced. When the incidence angle exceeds 80°, the number of vacancies decreases rapidly. This is mainly due to the larger incident angle is equivalent to the injection of parallel target surface, and the damage in the target is obviously reduced.

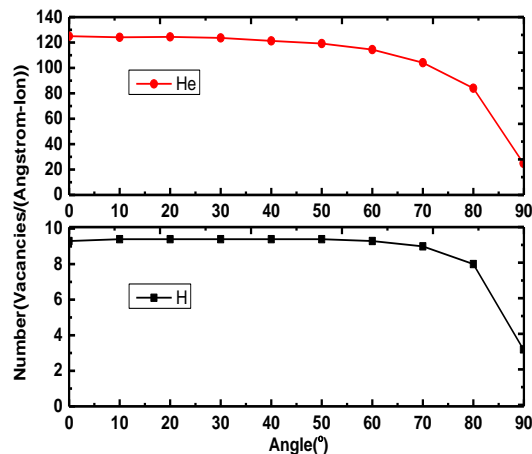


Fig. 8. Effect of the incident angle on the vacancies.

In order to study the sputtering phenomenon on CsPbBr₃ surface during ion irradiation, the relationship between sputtering yield and incidence angle was simulated, as shown in Figure 9. It can be seen from the figure that the sputtering yield increases with the increase of incident angle. When the incident angle is small, the cascade expansion is carried out longitudinally in the target. With the increase of incident angle, the cascade expansion is carried out horizontally in parallel to the target plane. Therefore, the sputtering yield increases with the increase of the number of cascading collisions within a certain depth.

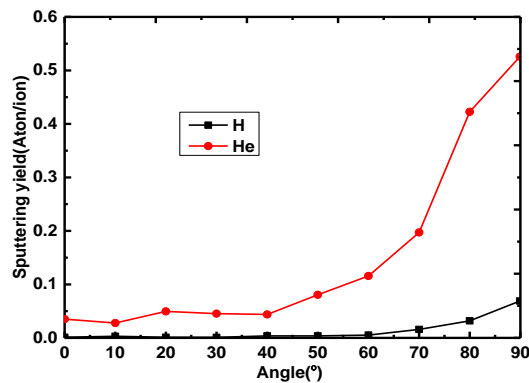


Fig. 9. Effect of the incident angle on the sputtering yield.

4. Conclusions

In summary, the effect of proton and He particle with different energies and angles on ion range, backscattering, vacancies and sputtering yield of CsPbBr₃ material was investigated by numerical simulation. The results show that the range and vacancies increased by increasing the particle energy. Meanwhile, the backscattering and sputtering yield gradually decreases with the increase of the particle energy. Also, It is clear that the the range and vacancies decrease and the sputtering yield by increasing the incident angles. Moreover, the degree of degeneration for all parameters induced by He particle were higher than that of proton. This is mainly due to the He particle is much heavier.

Acknowledgements

This research was funded by the Key Scientific Research Projects of Colleges and Universities in Henan Province (No.21B140006, 22A510016), Project funded by China Postdoctoral Science Foundation (No.2021M700685), National Scientific Research Project Cultivation Fund of Huanghuai University (No. XKPY-202103, XKPY-202106, XKPY-202006), the Award Plan for Tianzhong Scholars of Huanghuai University in 2019.

References

- [1] M. T. Hörantner, T. Leijtens, M. E. Ziffer, G. E. Eperon, M. G. Christoforo, M. D. McGehee, *ACS Energy Letters* 2(10), 2506 (2017); <https://doi.org/10.1021/acsenergylett.7b00647>
- [2] K. A. Bush, K. Frohna, R. Prasanna, R. E. Beal, T. Leijtens, S. A. Swifter, M. D. McGehee, *ACS Energy Letters* 3(2), 428 (2018); <https://doi.org/10.1021/acsenergylett.7b01255>
- [3] C. L. Li, C. Han, Y. B. Zhang, Z. G. Zang, M. Wang, X. S. Tang, J. H. Du, *Solar Energy Materials and Solar Cells* 172, 341 (2017); <https://doi.org/10.1016/j.solmat.2017.08.014>
- [4] T. T. Wang, W. T. Yang, B. Li, R. M. Bian, X. H. Jia, H. R. Yu, L. Wang, X. J. Li, F. Xie, H. P. Zhu, J. Q. Yang, Y. N. Gao, Q. Zhou, C. H. He, X. Y. Liu, Y. Ye, *ACS Applied Nano Materials* 3, 12017 (2020); <https://doi.org/10.1021/acsnm.0c02543>
- [5] N. J. Jeon, H. Na, E. H. Jung, T. Y. Yang, Y. G. Lee, G. Kim, H. W. Shin, S. II Seok, J. Lee, J. Seo, *Nature Energy* 3(8), 682 (2018); <https://doi.org/10.1038/s41560-018-0200-6>
- [6] K. Otte, L. Makhova, A. Braun, I. Konovalov, *Thin Solid Films* 613, 511 (2006); <https://doi.org/10.1016/j.tsf.2005.11.068>
- [7] V. V. Brus, F. Lang, J. Bundesmann, S. Seidel, A. Denker, B. Rech, G. Landi, H. C. Neitzert, J. Rappich, N. H. Nickel, *Advanced Electronic Materials* 3(2), 1600438 (2017); <https://doi.org/10.1002/aelm.201600438>
- [8] F. Lang, N. H. Nickel, J. Bundesmann, S. Seidel, A. Denker, S. Albrecht, V. V. Brus, J. Rappich, B. Rech, G. Landi, H. C. Neitzert, *Advanced Materials* 28(39), 8726 (2016); <https://doi.org/10.1002/adma.201603326>
- [9] C. C. Stoumpos, C. D. Malliakas, J. A. Peters, Z. Liu, M. Sebastian, J. Im, T. C. Chasapis, A. C. Wibowo, D. Y. Chung, A. J. Freeman, B. W. Wessels, M. G. Kanatzidis, *Crystal Growth Design* 13, 2722 (2013); <https://doi.org/10.1021/cg400645t>
- [10] L. Ding, S. N. Liu, Z. L. Zhang, G. Z. Shao, W. D. Xiang, X. J. Liang, *Ceramics International* 45(17), 22699 (2019); <https://doi.org/10.1016/j.ceramint.2019.07.307>
- [11] Q. A. Akkerman, M. Gandini, F. di Stasio, P. Rastogi, F. Palazon, G. Bertoni, M. J. Ball, M. Prato, A. Petrozza, L. Manna, *Nature Energy* 2(2), 16194 (2017); <https://doi.org/10.1038/nenergy.2016.194>
- [12] N. Dahbi, R. B. Talbe, O. Zaoui, *Journal of Ovonic Research* 15(3), 167 (2019).
- [13] M. El Marsi, R. Moulitif, S. Lahlou, S. Rochd, A. Dezairi, *Nuclear Instruments, and Methods in Physics Research B* 430, 72 (2018); <https://doi.org/10.1016/j.nimb.2018.05.046>
- [14] S. X. Sun, Y. H. Zhong, R. X. Yao, F. J. Cen, Y. X. Li, *Digest Journal of Nanomaterials and Biostructures* 15(4), 1089 (2020).
- [15] S. I. Radwan, M. M. Shehata, H. El-Khabeary, A. G. Helal, *Radiation Physics and Chemistry* 121, 93 (2016); <https://doi.org/10.1016/j.radphyschem.2015.12.019>
- [16] M. El Marsi, A. Guennoun, O. Elhaitamy, A. Dezairi, *Journal of Radioanalytical and Nuclear Chemistry* 326, 1579 (2020); <https://doi.org/10.1007/s10967-020-07440-x>
- [17] B. K. Durant, H. Afshari, S. Singh, B. Rout, G. E. Eperon, I. R. Sellers, *ACS Energy Letters* 6, 2362 (2021); <https://doi.org/10.1021/acsenergylett.1c00756>